Br J Dermatol 2024; **191**:580–591
https://doi.org/10.1093/bjd/ljae224
Advance access publication date: 30 May 2024

BJD
British Journal of Dermatology
Translational Research

Spatial transcriptomic analysis of amelanotic acral melanoma versus pigmented acral melanoma reveals distinct molecular determinants

Myoung Eun Choi,[1] Eun Ji Choi,[1] Jeong Hyeon Lee,[2] Chong Hyun Won,[1] Sung Eun Chang,[1] Mi Woo Lee[1] and Woo Jin Lee[1]

[1]Department of Dermatology, Asan Medical Center, University of Ulsan College of Medicine, Seoul, Republic of Korea
[2]Department of Biomedical Science, Bio-Medical Institute of Technology (BMIT), University of Ulsan College of Medicine, Ulsan, Korea
Correspondence: Woo Jin Lee. Email: uucm79@hanmail.net

Abstract

Background Amelanotic acral melanoma (AAM) is a rare type of acral melanoma that has a poor prognosis.

Objectives To investigate the transcriptomic differences between AAM and pigmented acral melanoma (PAM).

Methods Differences in the spatially resolved transcriptomic profiles of 9 patients with AAM with 29 regions of interest (ROIs) and 11 patients with PAM with 46 ROIs were investigated using S100b and CD3 morphology markers.

Results In S100b$^+$ tumour cell areas, we detected 11 upregulated differentially expressed genes (DEGs; including chaperone/ubiquitin-associated DEGs) and 82 downregulated DEGs (including human leucocyte antigen) in AAMs vs. PAMs. Protein–protein interaction network and pathway analyses revealed significant enrichment of dysregulated translational and nonsense-mediated decay pathways but significant decreases in antigen processing and presentation, interferon signalling and melanin biosynthesis pathways in S100b$^+$ ROIs of AAMs compared with PAMs. In tumour-associated immune cell areas, the numbers of CD8 T cells ($P=0.04$) and M1 macrophages ($P=0.01$) were significantly decreased, whereas those of monocytes ($P=0.04$) and endothelial cells ($P=0.04$) were increased in AAMs compared with PAMs.

Conclusions These findings could widen our understanding of the biological differences between AAMs and PAMs, which might result in a different clinical course.

Lay summary

Melanoma is one of the most serious types of skin cancer. As melanoma starts in cells that produce melanin (the substance that produces hair, eye and skin colouration), melanoma tumours are usually brown or black. 'Amelanotic melanoma' is a subtype of melanoma that has little or no melanin pigmentation. Less than 2% of melanomas are amelanotic melanomas. 'Acral melanoma' is a type of melanoma that occurs on the hands and feet. In acral melanoma, the lack of pigmentation has been associated with worse outcomes for patients. Why amelanotic acral melanoma (or 'AAM') has a worse prognosis than pigmented acral melanoma (or 'PAM') is unclear.

Using a type of technology called 'spatial transcriptomic analysis', we analysed a type of nucleic acid called RNA in 9 people with AAM and 11 with PAM. Seventy-five 'regions of interest' were selected. These regions of interest are known to be associated with tumour cells or immune cells around tumours.

We found that pathways involved in making proteins (translation) and in a process that removes faulty proteins called 'messenger RNA' were more active in AAM. However, pathways involved in processing and presenting antigens (substances that can trigger an immune response), the signalling of other proteins called 'interferons' and melanin production were less active in AAM. The number of specific types of white blood cells that recognize and attack tumours were decreased, whereas other cell types such as cells that line blood vessels were increased in AAM.

Our findings could increase our understanding of the differences between AAMs and PAMs. This may lead to an improvement in prognosis.

What is already known about this topic?

- Amelanotic melanoma is a rare type of cutaneous melanoma that is associated with a poorer prognosis than pigmented melanoma.
- In acral melanomas, amelanosis is an independent negative prognostic factor, even after adjusting for Breslow thickness and sex.

Accepted: 18 May 2024

What does this study add?

- Spatial transcriptomic analysis of amelanotic acral melanoma (AAM) revealed significant enrichment of translational and nonsense-mediated decay pathways and a significant decrease in antigen processing and presentation and interferon signalling compared with pigmented acral melanoma (PAM).
- Monocyte and endothelial cell counts were increased, whereas $CD8^+$ T-cell and M1 macrophage counts were significantly decreased in AAM compared with PAM.

What is the translational message?

- This study increases our understanding of the differences in transcriptomic expression and tumour microenvironment between AAM and PAM.
- The transcriptomic knowledge of AAM could contribute to the development of novel therapeutic strategies to improve the prognosis of AAM.

Cutaneous amelanotic melanoma refers to an amelanotic or hypomelanotic subtype of melanoma that exhibits no or little melanin pigmentation on examination or histological evaluation; the incidence varies from 0.4% to 27.5%.[1–4] Prompt recognition and early diagnosis of amelanotic melanomas are important, as patients with amelanotic melanoma are susceptible to misdiagnosis and have low survival outcomes vs. patients with cutaneous pigmented melanoma.[1,5–8] Previous studies have shown that amelanotic melanomas are associated with older age, Fitzpatrick skin type I and oculocutaneous albinism.[5,9–12] Histopathologically, amelanotic melanomas are characterized by thicker Breslow depth, more frequent ulceration and higher mitotic rates than pigmented melanomas, and they consist of a greater proportion of nodular, desmoplastic and acral lentiginous melanoma subtypes.[5,10,13,14]

The reasons behind the poor prognosis of amelanotic melanomas are not entirely clear. Some authors have suggested that amelanotic melanomas are frequently diagnosed at an advanced stage, due to higher misdiagnosis rates, which leads to low survival outcomes.[6,10,15] However, a study of acral melanomas reported that amelanosis was an independent negative prognostic factor, even after adjusting for Breslow thickness and sex.[13] Furthermore, amelanotic melanomas correlated independently with high mitotic rates and growth rates and ulcerated frequently, even after stratification by Breslow depth, implying their intrinsic aggressiveness.[5] Owing to the limited number of studies, the distinct biological features and mechanisms underlying the aggressiveness of amelanotic melanomas remain largely unknown.

Interestingly, acral melanoma – the most frequent melanoma subtype found in Asian countries – consists of a higher proportion of amelanotic melanomas than other subtypes, and amelanosis was identified as an independent factor for worse prognosis.[13,14,16] As the pathogenesis of and immune cell reactions against the tumour have been considered to be different in acral melanoma than in other subtypes, we aimed to investigate the differences in amelanotic melanoma and pigmented melanoma within the subtypes of acral melanoma.[7,17] Because traditional bulk RNA sequencing (RNAseq) cannot discriminate between the genetic expression of melanoma cancer cells from that of tumour-surrounding cells, we adopted spatially resolved transcriptomic profiling of specific tissues and cell populations, which enabled us to analyse the genetic expression of areas of interest using various morphology markers.[18] Therefore, we explored the genetic differences in amelanotic acral melanoma (AAM) and pigmented acral melanoma (PAM) using the cutting-edge method of spatial transcriptomic profiling.

Materials and methods

Patient selection and information

We defined AAMs as primary cutaneous acral melanomas that were both clinically and histopathologically devoid of pigmentation. The clinical data of 9 patients with AAM [2 with nail unit melanoma (NUM) and 7 with non-nail unit acral melanoma (NNUM)] and 11 with PAM (4 NUM and 7 NNUM) were retrieved (January 2016–July 2022) from electronic medical records and photographs at the Department of Dermatology, Asan Medical Center, Seoul, Republic of Korea (Table S1; see Supporting Information). The clinical and histopathological features, including median Breslow thickness, TNM stage and American Joint Committee on Cancer (AJCC) stage, were not significantly different between AAM and PAM. Patients' pathological data were extracted from histopathological and immunohistochemistry (IHC) slides, and staging was based on the 8th edition of the AJCC system.

Spatial transcriptome profiling

Formalin-fixed paraffin-embedded tumour tissues of 7 μm thickness were obtained from 20 patients with acral melanoma (Figure 1). The tissue samples were stained with large panels of premixed biological probes containing a unique ultraviolet (UV)-cleavable DNA oligonucleotide barcode. Three fluorescence-labelled morphological markers (S100b, CD3, DNA) were used to elucidate visually the tissue boundary and select the regions of interest (ROIs). We selected ROIs based on morphological marker intensity. The maximum ROI size was 100 000 μm^2 and the minimum nuclei count was 50. We selected 16 and 24 $S100b^+$ ROIs (tumour cell areas) from AAM and PAM samples, respectively (Figure 2a). We also selected 13 and 22

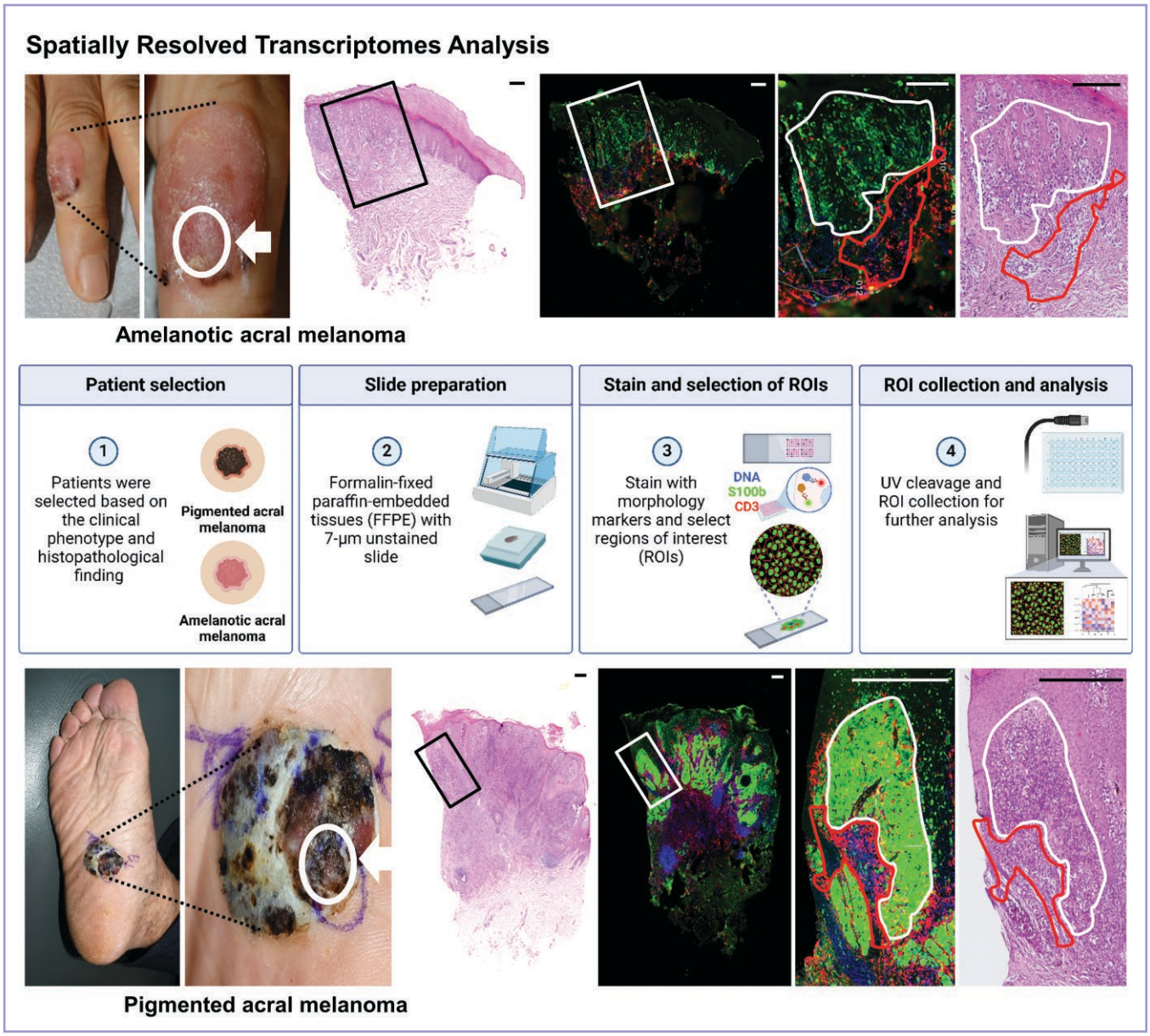

Figure 1 Spatially resolved transcriptomic analysis workflow. Representative photographs of amelanotic melanoma (AAM), pigmented acral melanoma (PAM) and their haematoxylin and eosin-stained slide images with matched digital spatial profiler images. The biopsy site is marked with the white arrow. Region of interest (ROI) selection process in AAM and PAM based on DNA (blue), S100b (green) and CD3 (red) morphology markers (scale bars = 300 μm). UV, ultraviolet.

S100b$^-$/CD3$^+$ ROIs (tumour-associated immune cell areas) from AAM and PAM samples, respectively (Figure 2a). UV illumination of 75 defined ROIs induced the release of ROI-tagged DNA barcode tags that were taken up by a micro-capillary system and dispensed into a 96-well microtitre plate for subsequent analysis using GeoMx® DSP analysis software version 2.1 (NanoString Technologies, Seattle, WA, USA; Figure 1).

We performed spatial transcriptomic profiling of samples using the GeoMx Human Whole Transcriptome Atlas Human RNA for Illumina Systems (NanoString Technologies), which included 18 676 genes. Sequencing quality for sufficient saturation, ensuring low-expressor sensitivity, was confirmed and normalized by the third quartile (Q3) for differences in cellularity and ROI size.

Region of interest-based gene expression analysis

For dimensional reduction, principal component analysis and uniform manifold approximation and projection (UMAP) using the dimension reduction DSP DA script (version 1.2) of the GeoMx DSP analysis software version 2.1 was performed in both S100b$^+$ and CD3$^+$ segments.

Differentially expressed genes (DEGs) were evaluated using the GeoMx DSP analysis software to calculate the fold-change and *P*-values between S100b$^+$ and CD3$^+$ ROIs of AAM and PAM samples. DEGs with fold-change thresholds >2 or <0.5 and a *P*-value <0.05 were screened out. All DEGs were displayed using a volcano map plotted using ggplot2 in R version 4.1.3 (R Foundation for Statistical Computing, Vienna, Austria).

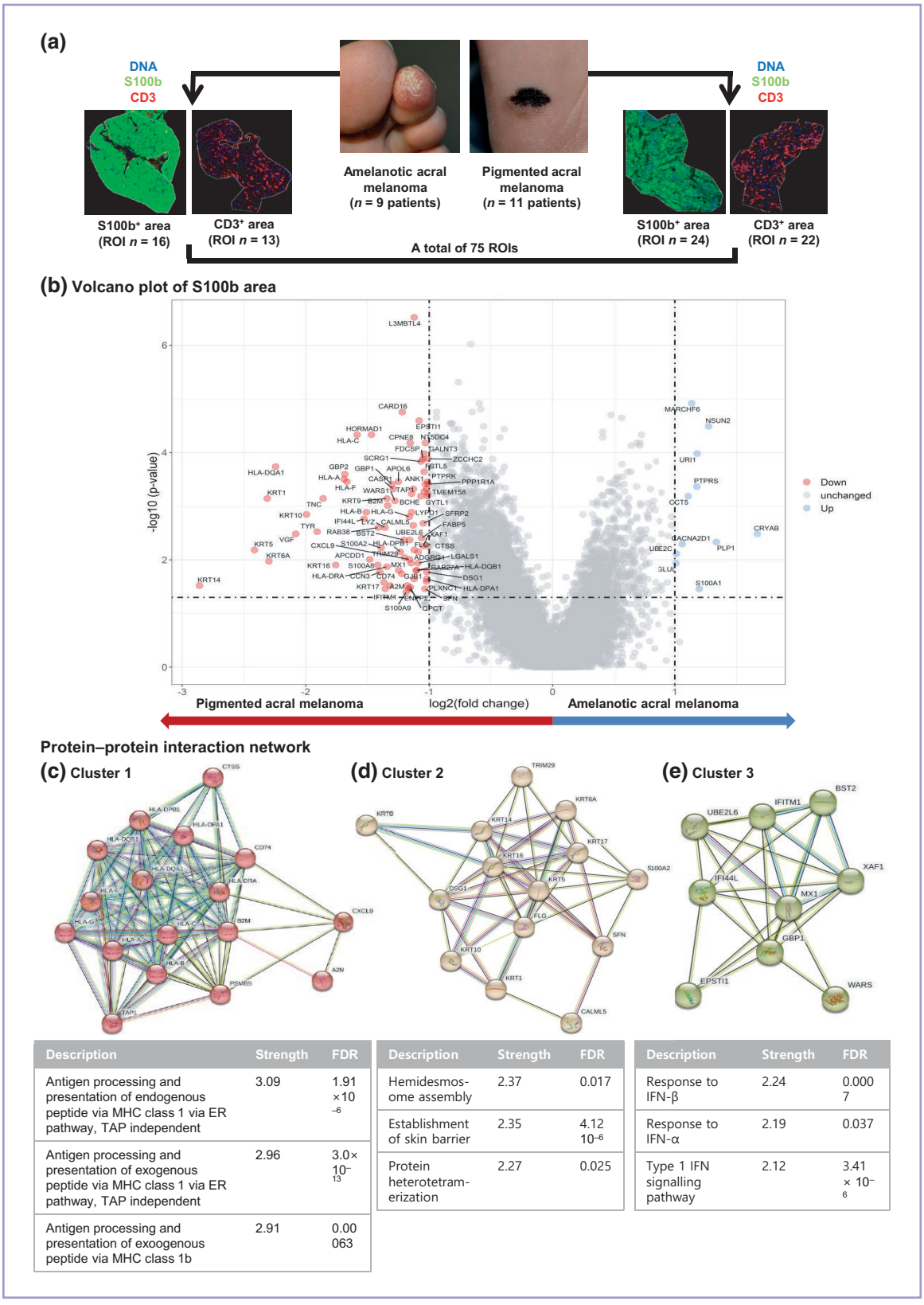

Description	Strength	FDR
Antigen processing and presentation of endogenous peptide via MHC class 1 via ER pathway, TAP independent	3.09	1.91×10^{-6}
Antigen processing and presentation of exogenous peptide via MHC class 1 via ER pathway, TAP independent	2.96	3.0×10^{-13}
Antigen processing and presentation of exogenous peptide via MHC class 1b	2.91	0.00063

Description	Strength	FDR
Hemidesmosome assembly	2.37	0.017
Establishment of skin barrier	2.35	4.12×10^{-6}
Protein heterotetramerization	2.27	0.025

Description	Strength	FDR
Response to IFN-β	2.24	0.0007
Response to IFN-α	2.19	0.037
Type 1 IFN signalling pathway	2.12	3.41×10^{-6}

Figure 2 Digital spatial transcriptomic analysis revealed that genetic expression differed between amelanotic acral melanoma (AAM) and pigmented acral melanoma (PAM). (a) Summary of the experimental design. (b) Volcano plot showing differentially expressed genes with fold changes > 2 and a *P*-value < 0.05 in S100b+ tumour cell areas. Protein–protein interaction network analysis revealed three separate clusters, including (c) a cluster of antigen processing and presentation, (d) a skin barrier-related cluster and (e) an interferon-associated cluster. ER, endoplasmic reticulum; FDR, false discovery rate; IFN, interferon; MHC, major histocompatibility complex; ROI, region of interest; TAP, transporter associated with antigen processing.

Protein–protein interaction (PPI) network analysis was conducted using the Search Tool for the Retrieval of Interacting Genes (https://string-db.org/) to evaluate the correlation between the protein products of DEGs. Functional enrichments of the network were based on the biological process of Gene Ontology (GO), and clustering was performed using the Markov cluster algorithm (MCL clustering).

Next, pathway analysis of S100b$^+$ and CD3$^+$ ROIs of AAM and PAM samples was conducted using the GeoMx DSP analysis software using a fast gene set enrichment analysis package for R (https://github.com/ctlab/fgsea) from the Bioconductor and Reactome database. Additional pathway analysis using DEGs was conducted using DAVID bioinformatics resources (https://david.ncifcrf.gov/). Pathways were described in biological process GO terms.

A gene set considered to be cell-type specific was analysed in CD3$^+$ areas, to determine the abundance of 14 immune cell populations (macrophages, mast cells, B cells, plasma cells, CD4$^+$ T cells, CD8$^+$ T cells, NK cells, plasmacytoid and myeloid dendritic cells, monocytes, neutrophils, regulatory T cells, endothelial cells and fibroblasts) using the GeoMx DSP analysis software. Moreover, we used CIBERSORTx (https://cibersortx.stanford.edu/) to calculate the abundance score for 22 immune cell types.

Immunohistochemistry

Ubiquitin-conjugating enzyme E2 C (UBE2C), crystallin alpha B (CRYAB), ubiquitin-conjugating enzyme E2 L6 (UBE2L6), XIAP-associated factor 1 (XAF1), guanylate binding protein 1 (GBP1), major histocompatibility complex class II DQ alpha 1 (HLA-DQ1), transporter associated with antigen processing 1 (TAP1) and pan-cytokeratin (panCK) were selected for IHC to confirm DEGs. Paraffin-embedded sections were immunostained with anti-UBE2C [1 : 50 (ab252940; Abcam, Cambridge, MA, USA)], anti-CRYAB [1 : 400 (ab13496; Abcam)], anti-UBE2L6 [1 : 5000 (ab109086; Abcam)], anti-XAF1 [1 : 500 (ab17204; Abcam)], anti-GBP1 [1:4000 (ab131255; Abcam)], anti-HLA-DQ1 [1 : 6000 (ab128959; Abcam)], anti-TAP1 [1 : 4000 (11114-1-AP; Proteintech, Chicago, IL, USA)] and anti-panCK [1 : 400 (NCL-L-AE1/AE3; Novocastra, Newcastle, UK)] antibodies. Moreover, to validate the results from immune cell deconvolution, we conducted IHC for anti-CD8 [1 : 100 (108M-96; Cell Marque, Rocklin, CA, USA)], anti-CD86 [1 : 1000 (ab53004; Abcam)] and anti-CD31 [1 : 100 (108M-96; Cell Marque)]. We used the independent acral melanoma cohort, which comprised 14 AAMs and 25 PAMs, for IHC. IHC intensity was rated 0–3 based on expression, using a semiquantitative method as follows: 0, 1, 2 and 3 indicated $<10\%$, 10–30%, 30–50% and $>50\%$, respectively, of total melanoma cell areas for DEG confirmation. The same parameter was used for the confirmation of immune cell deconvolution, except that the total area was calculated based on the immune cell-infiltrated area. The results of IHC staining were evaluated by two independent dermatologists (W.J.L. and M.E.C.) at $\times 100$ magnification.

Single-cell RNA sequencing using public database

Single-cell RNAseq (scRNAseq) was conducted for external validation using one AAM sample (stored in Github: https://github.com/TianJie327/acral-amelanotic-melanoma) and 4 PAM samples from GSE215121. The data from all samples were loaded in R (version 4.3.2) using the Read10X function from the Seurat package (version 5), followed by creating an aggregated gene expression matrix and Seurat object. We used the FindClusters function on 24 principal components with a resolution of 0.7 to perform the cluster analysis. We used *MLANA*, *PMEL* and *MITF* activity for melanoma cluster annotation. DEG analysis adopted the pseudobulk approach and used DEseq2 for DEG analysis. Additional pathway analysis with common DEGs was performed using DAVID bioinformatic resources.

Statistical analysis

Gene expression in AAM and PAM samples was compared using an independent Student's *t*-test and Mann–Whitney *U* test. Two-sided *P*-values <0.05 were considered to be statistically significant. Multiple hypothesis testing in every analysis was controlled using the Benjamini–Hochberg procedure. A false discovery rate cutoff of <0.05 was the significance threshold. IHC staining results were analysed using a χ^2 or Fisher's exact test comparing low (IHC staining intensity of 0–1) and high (IHC staining intensity of 2–3) expression. Statistical analysis was conducted using R version 4.1.3.

Results

Dimension reduction plot

The UMAP results showed that AAM and PAM did not form separate clusters in either S100b$^+$ and CD3$^+$ segments (Figure S1a, b; see Supporting Information). Additionally, UMAP based on individual patients implied intratumoral heterogeneity.

Differentially expressed genes in amelanotic acral melanoma and pigmented acral melanoma

In S100b$^+$ areas (tumour cell areas), we found that 93 genes were significantly differently expressed in AAMs compared with PAMs; these included 11 upregulated and 82 downregulated DEGs [Figure 2b, Table S2 (see Supporting Information)]. Approximately half of the upregulated DEGs were associated with chaperone/chaperonin (*CCT5*, *URI1*, *CRYAB*) and ubiquitin (*UBE2C*, *MARCHF6*). PPI network analysis and clustering of downregulated DEGS, which was performed to analyse the functions and relations of the 82 downregulated DEGs, revealed 4 main clusters. The first 17 DEGs (*CTSS*, *HLA-DPB1*, *HLA-DQB1*, *HLA-DPA1*, *HLA-DQA1*, *HLA-DRA*, *HLA-A*, *HLA-B*, *HLA-C*, *HLA-F*, *HLA-G*, *CD74*, *A2 M*, *B2 M*, *CXCL9*, *PSMB9*, *TAP1*) were associated with antigen processing and presentation (Figure 2c), the next 14 (*KRT1*, *KRT5*, *KRT6A*, *KRT9*, *KRT10*, *KRT14*, *KRT16*, *KRT17*, *FLG*, *SFN*, *DSG1*, *S100A2*, *TRIM29*, *CALML5*) were associated with the skin barrier (Figure 2d) and the next 9 (*UBE2L6*, *IFITM1*, *BST2*, *IFI44L*, *MX1*, *XAF1*, *GBP1*, *EPSTI1*, *WARS*) were associated with the interferon (IFN) pathway (Figure 2e). The fourth main cluster, which included five genes (*TYR*, *BCHE*, *RAB38*, *SLC24A5*, *RAB27A*), was

associated with melanin biosynthesis and expected to be downregulated in AAMs vs. PAMs. Functional analysis based on DEGs is presented in Figure S2.

To assess intratumoral heterogeneity, we evaluated *z*-scores from DEGs involved in these main clusters, in addition to chaperone (*CCT5*, *URI1*, *CRYAB*) and ubiquitin (*UBE2C*, *MARCHF6*) genes, which showed modest variation across individual ROIs (Figure 3a). Furthermore, different ROIs from the same tumour revealed different gene expression levels related to melanogenesis (Figure 3b).

We evaluated the expression of keratin 1 (KRT1) and keratin 10 (KRT10) in S100b areas, which revealed four ROIs with high KRT1/KRT10 expression, because of possible keratinocyte contamination due to close spatial overlap between

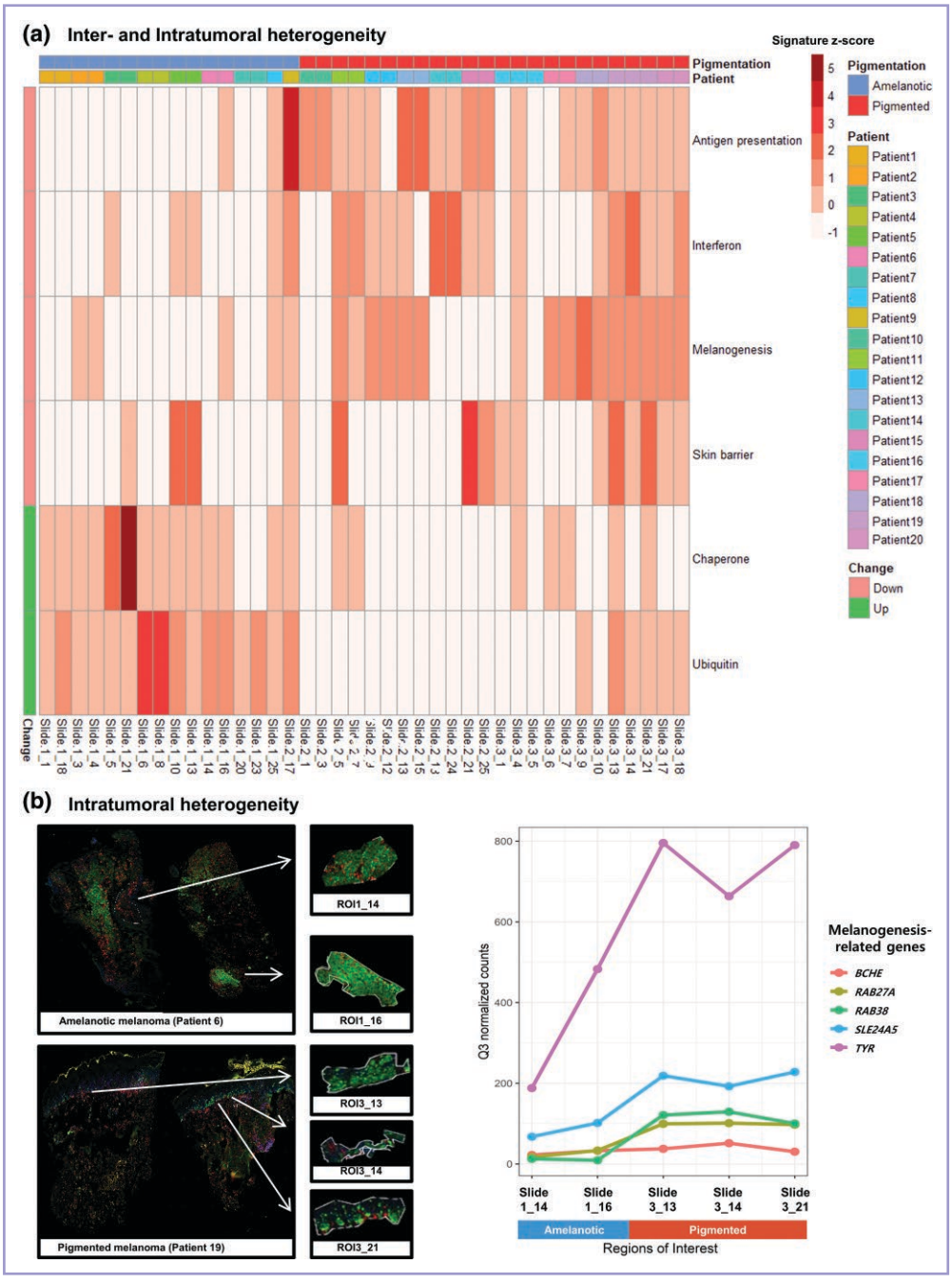

Figure 3 Inter- and intratumoral heterogeneity. (a) Heatmap of 40 regions of interest (ROIs) from 20 individual tumours highlighting the main gene signatures from differentially expressed genes (DEGs). Results are presented according to colour scale with gene signature *z*-scores. The antigen presentation cluster included 17 DEGs (*CTSS*, *HLA-DPB1*, *HLA-DQB1*, *HLA-DPA1*, *HLA-DQA1*, *HLA-DRA*, *HLA-A*, *HLA-B*, *HLA-C*, *HLA-F*, *HLA-G*, *CD74*, *A2 M*, *B2 M*, *CXCL9*, *PSMB9*, *TAP1*); the interferon cluster included 9 DEGs (*UBE2L6*, *IFITM1*, *BST2*, *IFI44L*, *MX1*, *XAF1*, *GBP1*, *EPSTI1*, *WARS*); the melanogenesis cluster included 5 DEGs (*TYR*, *BCHE*, *RAB38*, *SLC24A5*, *RAB27A*); the skin barrier cluster included 14 DEGs (*KRT1*, *KRT5*, *KRT6A*, *KRT9*, *KRT10*, *KRT14*, *KRT16*, *KRT17*, *FLG*, *SFN*, *DSG1*, *S100A2*, *TRIM29*, *CALML5*); the chaperon cluster included 3 DEGs (*CCT5*, *URI1*, *CRYAB*); and the ubiquitin cluster included 2 DEGs (*UBE2C*, *MARCHF6*). (b) Two ROIs from a patient with amelanotic melanoma (patient 6) and three ROIs from a patient with pigmented melanoma (patient 19) were used to show intratumoral heterogeneity. Comparison of transcript levels of melanin biosynthesis genes are presented with $\log_2$Q3 normalized counts.

malignant melanocytes and keratinocytes (Figure S3a; see Supporting Information). DEG analysis excluding these 4 ROIs revealed that 69 genes were differentially expressed between AAMs and PAMs. Ten genes were significantly upregulated, including *CCT5*, *UBE2C* and *MARCHF6*, while 59 were significantly downregulated [Figure S3b, Table S3 (see Supporting Information)]. The PPI network analysis with downregulated DEGs showed three main clusters with melanin biosynthesis (*KIT*, *OCA2*, *RAB27A*, *RAB38*, *SLC24A5*, *STXBP1*, *TYR*), IFN signalling (*UBE2L6*, *IFITM1*, *BST2*, *IFI44L*, *IFI6*) and antigen processing and presentation (*B2M*, *HLA-A*, *HLA-C*, *HLA-F*, *HLA-G*) (Figure S3c–e).

The list of DEGs in $CD3^+$ areas (tumour-associated immune cell areas) is provided in Figure S1(c) and Table S2. The list of DEGs according to age, sex, tumour location, Breslow thickness, ulceration and mitotic rate is presented in Table S4 (see Supporting Information). Additionally, Figure S4 (see Supporting Information) shows the pathway analysis based on these DEG lists.

Pathway analysis of amelanotic acral melanoma vs. pigmented acral melanoma

Pathway analysis was conducted with the exclusion of ROIs expressing high KRT1/KRT10 and showed that 302 pathways were significantly upregulated and 42 significantly downregulated in AAMs compared with PAMs (Figure 4). The upregulated pathways included eukaryotic translation initiation [normalized enrichment score (NES) = 8.28, adjusted *P* (P_{adj}) = 0.003)], cap-dependent translation initiation (NES = 8.28, P_{adj} = 0.003), L13a-mediated translational silencing of ceruloplasmin expression (NES = 8.27, P_{adj} = 0.003), guanosine triphosphate hydrolysis and joining of the 60S ribosomal subunit (NES = 8.20, P_{adj} = 0.003), and nonsense-mediated decay independent of the exon junction complex (NES = 7.80, P_{adj} = 0.003). The representative downregulated pathways included IFN-α/β signalling (NES = −4.85, P_{adj} = 0.003), IFN-γ signalling (NES = −4.68, P_{adj} = 0.003), IFN signalling (NES = −4.48, P_{adj} = 0.003), class A/1 rhodopsin-like receptors (NES = −4.34, P_{adj} = 0.003), chemokine receptors bind chemokines (NES = −3.79, P_{adj} = 0.003) and immunoregulatory interactions between lymphoid and nonlymphoid cells (NES = −3.61, P_{adj} = 0.003). The detailed pathways that were significantly different between AAMs and PAMs are provided in Table S5 (see Supporting Information), while Table S6 (see Supporting Information) shows the list of genes that were included in the representative Reactome pathways. Furthermore, Table S7 (see Supporting Information) provides the pathway analysis results, including all ROIs.

Immune cell deconvolution

In the immune cell deconvolution analysis using the GeoMx DSP profiler, we found that the number of endothelial cells was statistically significantly increased in AAMs compared with PAMs (*P* = 0.04; Figure 5a). For a specific analysis of immune cell types, we employed CIBERSORTx, which revealed that the numbers of $CD8^+$ T cells (*P* = 0.04) and M1 macrophages (*P* = 0.01) were significantly decreased, whereas the number of monocytes (*P* = 0.04) was significantly increased in AAMs compared with PAMs (Figure 5b).

Immunohistochemistry

Among chaperone/ubiquitin-related proteins, the expression of UBE2C was similar between AAMs and PAMs (*P* = 0.75; Figure 6a), while CRYAB was more frequently stained in AAMs (*P* = 0.03; Figure 6b). However, UBE2L6 (*P* = 0.005), XAF1 (*P* = 0.003) and GBP1 (*P* = 0.01) – proteins related to interferon signalling – were significantly more intensely stained in PAMs compared with AAMs (Figure 6c–e).

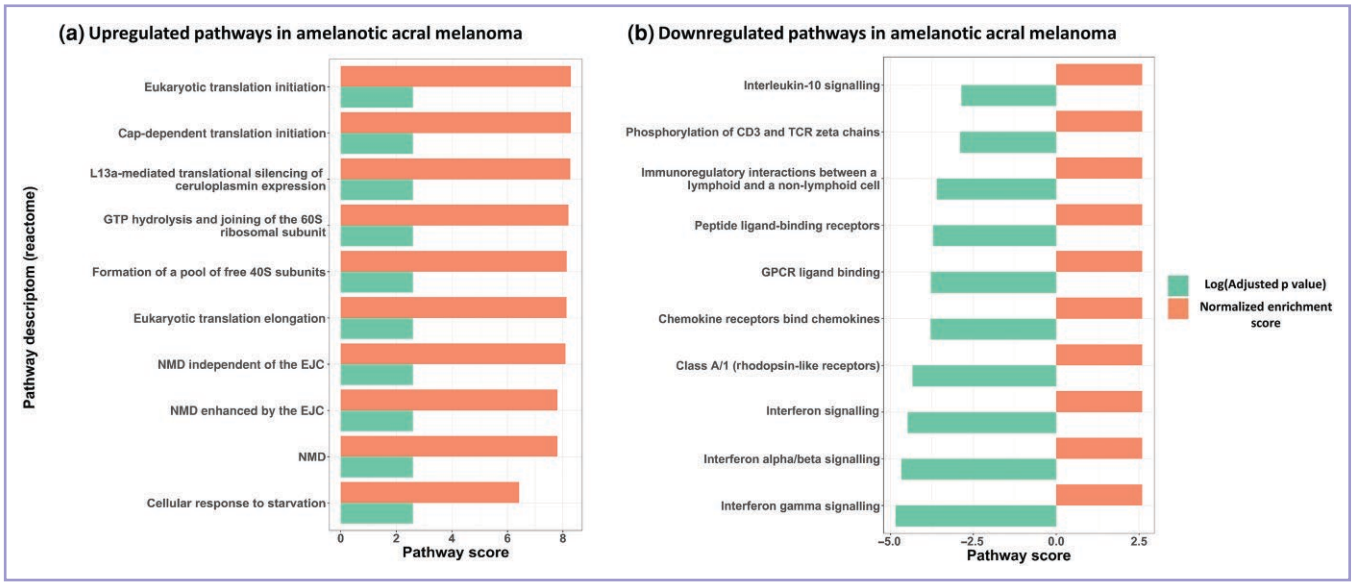

Figure 4 Representative pathways with normalized enrichment score and $-\log_{10}$(adjusted *P*-value) that were significantly different between amelanotic acral melanoma (AAM) and pigmented acral melanoma (PAM) analysed by digital spatial profiling. (a) Upregulated pathways included dysregulated translation and nonsense-mediated decay (NMD)-associated pathways, and (b) downregulated pathways included interferon signalling, keratinization and others. EJC, exon junction complex; GPCR, G protein-coupled receptor; GTP, guanosine triphosphate; NMD, nonsense-mediated decay; TCR, T-cell receptor.

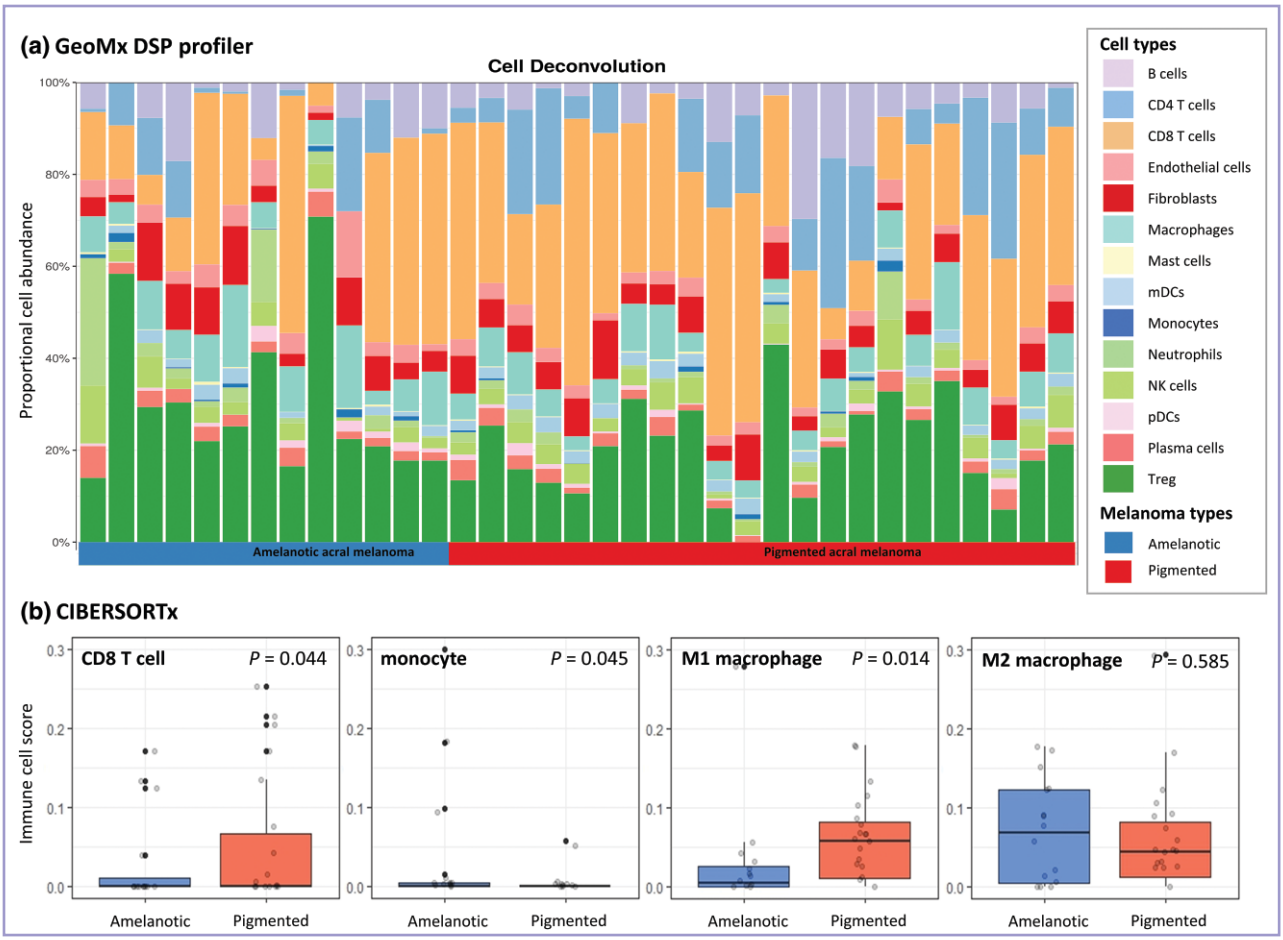

Figure 5 Immune cell profiling of amelanotic acral melanoma (AAM) and pigmented acral melanoma (PAM). (a) Diagram of cell composition of 35 $CD3^+$ regions of interest (tumour-associated immune cell areas) analysed with GeoMx® DSP analysis software version 2.1. (b) Pairwise box plots of immune cell scores (CD8 T cells, monocytes, M1 macrophages and M2 macrophages) determined by CIBERSORTx (https://cibersortx.stanford.edu/). mDC, myeloid dendritic cell; NK, natural killer; pDC, plasmacytoid; Treg, regulatory T cell.

Furthermore, proteins associated with antigen presentation and processing [HLA-DQA1 ($P=0.03$) and TAP1 ($P=0.02$)] were also significantly more intensely stained in PAMs compared with AAMs (Figure 6f–g). As panCK was stained within the epidermal layer, we assessed the IHC staining of invasive AAMs and PAMs only in the dermis. None of the invasive AAMs was stained with panCK, while 43% of invasive PAMs were stained with panCK in the dermal tumour area [Figure 6h; Figure S5 (see Supporting Information)].

CD8 and CD86 were more frequently stained in PAMs vs. AAMs [$P=0.03$ and $P=0.06$, respectively; Figure S6a, b (see Supporting Information)]. AAMs were more frequently stained with CD31 than PAMs (57.2% vs. 32.0%), but this was not statistically significant ($P=0.13$; Figure S6c).

Single-cell RNA sequencing using a public database

We found that two upregulated (*CACNA2D1*, *PTPRS*) and 14 downregulated DEGs (*KRT10*, *HORMAD1*, *RAB38*, *LYZ*, *IFITM1*, *KRT9*, *ENPP2*, *HLA-G*, *MX1*, *TAP1*, *EPSTI1*, *FSTL5*, *ANK1*, *PSMB9*) in AAM vs. PAM were also included in the list of DEGs in scRNAseq using the public database Gene Expression Omnibus (GEO). Pathways using these DEGs also included antigen presentation and process pathways, IFN signalling pathways and the intermediate filament organization pathway (Figure S7; see Supporting Information).

Discussion

Although most studies have found that amelanosis is associated with lower survival outcomes, the reasons for the higher mortality seen in AM have not been widely investigated.[5,7,8,19] A previous murine model study demonstrated that amelanotic melanomas are characterized by the expression of epithelial–mesenchymal transition-like and transforming growth factor-β signatures.[20] Furthermore, another study using mass spectrometry-based proteomics revealed that a set of proteins involved in cell adhesion/migration was highly expressed in metastatic amelanotic melanomas vs. metastatic pigmented melanomas.[21] Nevertheless, melanoma is one of the most heterogeneous cancers, and acral melanoma has unique characteristics of a higher proportion of amelanotic melanomas and fewer UV signature mutations than other subtypes.[13,14,16,22–24] Therefore, we investigated the genetic differences based on amelanosis within the acral melanoma subtype.

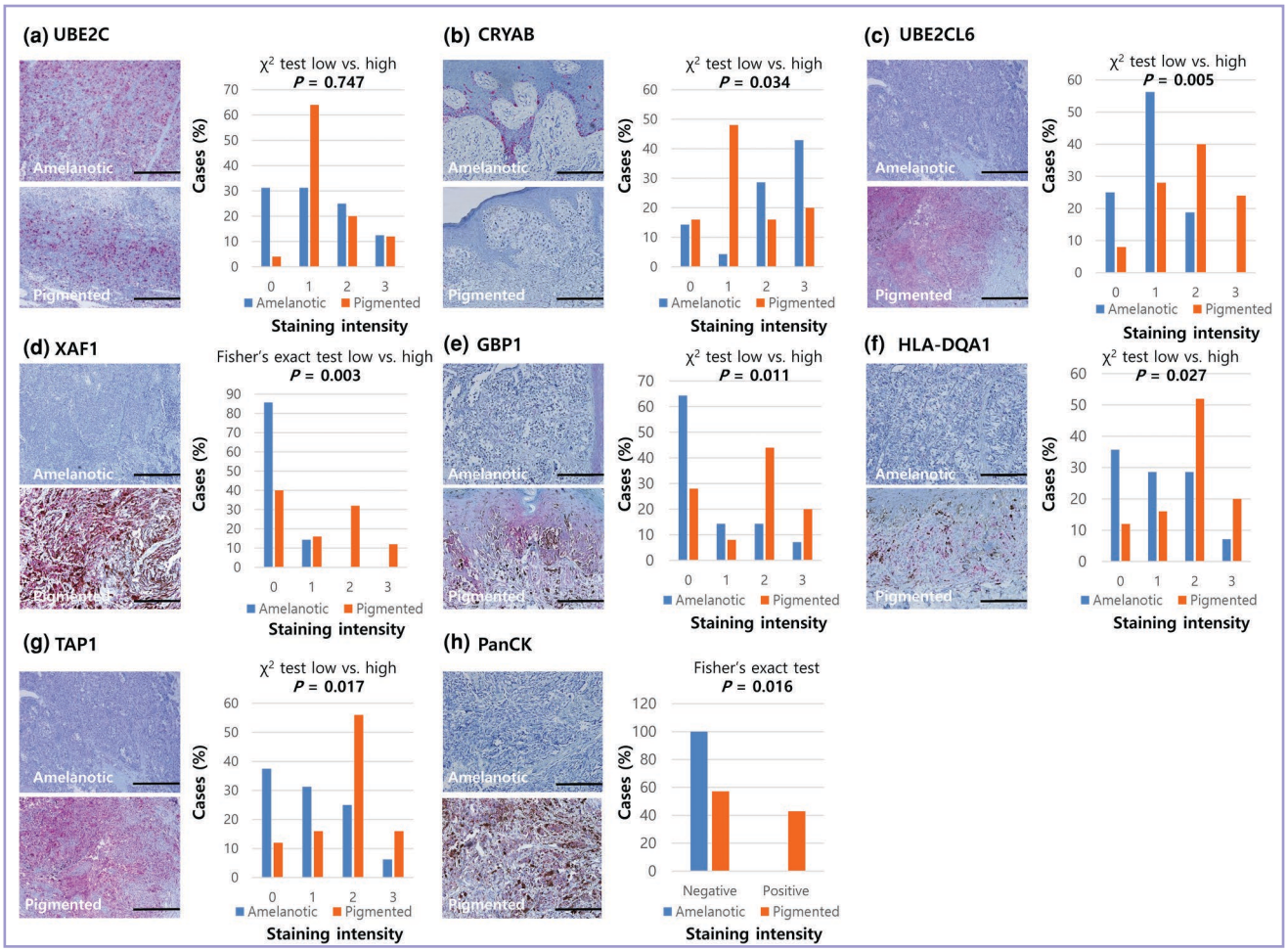

Figure 6 Immunohistochemistry results of amelanotic acral melanoma (AAM) and pigmented acral melanoma (PAM). (a) Ubiquitin-conjugating enzyme E2 C (UBE2C), (b) crystallin alpha B (CRYAB), (c) ubiquitin-conjugating enzyme E2 L6 (UBE2L6), (d) XIAP-associated factor 1 (XAF1), (e) guanylate binding protein 1 (GBP1), (f) major histocompatibility complex class II DQ alpha 1 (HLA-DQA1), (g) transporter associated with antigen processing 1 (TAP1) and (h) pan-cytokeratin (panCK). Magnification in (a), (c) and (g)×100 (scale bar=200 μm); magnification in (b), (d), (e), (f) and (h)×200 (scale bar=100 μm).

In the DEG analysis, we found that several chaperone-associated (*URI1*, *CCT5*, *CRYAB*) and ubiquitin-associated (*UBE2C*) genes were upregulated in AAMs vs. PAMs. Molecular chaperones are proteins that assist with the conformational folding or unfolding of large proteins, and play pivotal roles in controlling protein quality.[25] Previous reports have supported the hypothesis that chaperones are implicated in antiapoptosis and have a role in the cell proliferation, invasiveness, angiogenesis, metastasis and immune tolerance of various cancers.[26–31] Hence, the overexpression of chaperones may be correlated with the poor prognosis of cancers, including melanoma.[32,33] In addition, UBE2C (a product of *UBE2C*) is essential for cell cycle progression through M phase and is thus involved in the tumorigenesis and progression of several types of cancers.[34–39]

The DEG and pathway analyses demonstrated that IFN signalling was significantly decreased in AAMs compared with PAMs. The importance of IFN signalling in melanoma has already been widely recognized, and pegylated IFN was frequently used as an adjuvant therapy in patients with advanced melanoma before the advent of immune checkpoint inhibitors (ICIs).[40] Furthermore, in our study, DEGs associated with the biological process of hemidesmosome assembly and skin barrier establishment were downregulated in AAMs vs. PAMs. We conducted panCK IHC staining with AE1/AE3 antibody and found that panCK was significantly more frequently stained in invasive PAM compared with invasive AAM in melanoma cells in the dermal tumour area, with scRNAseq of the GEO public database confirming the result. However, we should be cautious interpreting keratin-related DEG data because of possible keratinocyte contamination in the tumour cell ROIs due to the close proximity to melanoma cells. Nevertheless, similar results were observed in DEGs and pathway analysis after excluding superficially located ROIs with high KRT1/KRT10 expression.

Furthermore, in the present study, several DEGs associated with human leucocyte antigen (HLA) genes were downregulated in AAMs vs. PAMs. Previous studies have revealed that decreased HLA gene expression is generally associated with lower immune cell infiltration, poorer survival in the majority of cancer types and lower response to ICIs.[41] Finally, we identified several downregulated melanogenesis-related DEGs in AAM (*TYR*, *BCHE*, *RAB38*, *SLC24A5*, *RAB27A*), while the RNA level of *MITF* was not

significantly different between AAM and PAM [log2(fold change) = −0.30; $P = 0.59$], consistent with the fact that melanocyte inducing transcription factor activity is mainly modulated by several factors at post-transcriptional and post-translational levels.[42] We also found that *RAB38* was significantly downregulated in AAM compared with PAM in scRNAseq of the GEO public database. Reflecting the role of RAB38 in the control of melanosome biogenesis and transport, downregulation of *RAB38* RNA expression could play significant role in the AAM phenotype.[42]

The cancer cell is characterized by unrestricted proliferation for which an increased rate of protein synthesis is requisite.[43] Eukaryotic translation initiation, which showed the highest pathway score in AAMs and not PAMs in this study, is the rate-limiting step and thus subject to regulation in cancers. We found that 199 pathways were significantly upregulated, whereas 32 pathways were significantly downregulated in both NUMs and NNUMs, and – interestingly – eukaryotic translation initiation was one of the most importantly upregulated pathways in both NUMs and NNUMs (Table S8; see Supporting Information). Dysregulation of translation is a critical driving force of tumorigenesis, as well as of tumour progression.[41] Furthermore, the components of the eukaryotic initiation factor-4F complex could mediate resistance to targeted therapies, as well as conventional chemotherapies in several cancers.[42,44–47] In addition, translational reprogramming is currently emerging as a key factor in melanoma plasticity, switching between proliferative and invasive phenotypes.[43,48,49]

Immune cell deconvolution revealed significantly decreased numbers of CD8 T cells and M1 macrophages but increased numbers of monocytes in AAMs compared with PAMs. The downregulated pathway of chemokine receptors bind chemokines in the S100b$^+$ segments, as well as several downregulated DEGs (*CXCL9, CCL19*) in the CD3$^+$ segments of AAMs could be closely linked to this observation. CD8 T cells and M1 macrophages induce an immune response against tumours, whereas the number of monocytes serves as a surrogate marker of high tumour burden.[50] In melanoma, the peripheral and intratumoral lymphocyte-to-monocyte ratio has been identified as an independent poor prognostic factor for survival, as well as a negative indicator of ICIs in melanoma.[51,52] We observed these changes in immune cell distribution in both total acral samples and NUMs but not in NNUMs (Figure S8; see Supporting Information). This finding could imply a different tumour microenvironment between NUMs and NNUMs; however, further studies are required to clarify this assumption. Moreover, we found that the number of endothelial cells in the GeoMx DSP profiler was statistically significantly increased in AAMs compared with PAMs. A recent study that analysed factors influencing the type of acral melanoma metastasis (first metastasis to lymph node vs. first distant metastasis) demonstrated that AAM was associated with first distant metastasis, whereas heavy pigmentation was associated with first lymph node metastasis.[53] The degree of pigmentation could impact on the pathway of tumour cell migration from the original site to a distant location; further studies are necessary to clarify the exact mechanism underlying this difference.

This study has several limitations. Firstly, the sample size of AAMs and PAMs was relatively small, because spatial transcriptome profiling techniques require the delicate selection of fresh tissues. Additionally, the number of ROIs was not equally selected per patient (2 ROIs for 16 patients, 1 ROI for 2 patients, and 3 ROIs for 2 patients) owing to differences in the immunofluorescence level of morphology makers. Moreover, despite the fact that spatial transcriptome profiling is a cutting-edge and advanced technique, it could not completely separate melanoma tumour cells from tumour-surrounding cells in close proximity. Although further analysis was conducted with the exclusion of ROIs expressing high KRT1 and KRT10, an admixture of keratinocytes in some ROIs could be a limitation of this study. We could not perform subgroup analysis based on melanoma location or amelanosis because of limited information.

In conclusion, AAMs were associated with increased dysregulated translation pathways in addition to protein quality control and chaperone DEGs and decreased IFN signalling, HLA-associated genes and melanin biosynthesis in addition to an immunosuppressive tumour microenvironment (Figure S9; see Supporting Information). This novel finding could widen our understanding of the pathophysiological differences between AAMs and PAMs, which might lead to different clinical features and survival outcomes.

Funding sources

This work was supported by a grant from the National Research Foundation of Korea (grant number: NRF-2021R1C1C1005392), which is funded by the Ministry of Science and Information Technology of the Korean government and a grant from the Asan Institute for Life Sciences, Asan Medical Center, Seoul, Korea (2023IF-0001-1).

Conflicts of interest

The authors declare no conflicts of interest.

Data availability

The data that support the findings of this study are available from the corresponding author upon reasonable request.

Ethics statement

This study was reviewed and approved by the Institutional Review Board (IRB) of the Asan Medical Center (approval no. 2021-0648).

Supporting Information

Additional Supporting Information may be found in the online version of this article at the publisher's website.

References

1 Cheung WL, Patel RR, Leonard A *et al.* Amelanotic melanoma: a detailed morphologic analysis with clinicopathologic correlation of 75 cases. *J Cutan Pathol* 2012; **39**:33–9.
2 Giuliano AE, Cochran AJ, Morton DL. Melanoma from unknown primary site and amelanotic melanoma. *Semin Oncol* 1982; **9**:442–7.

3 Menzies SW, Kreusch J, Byth K *et al.* Dermoscopic evaluation of amelanotic and hypomelanotic melanoma. *Arch Dermatol* 2008; **144**:1120–7.
4 Gong HZ, Zheng HY, Li J. Amelanotic melanoma. *Melanoma Res* 2019; **29**:221–30.
5 Moreau JF, Weissfeld JL, Ferris LK. Characteristics and survival of patients with invasive amelanotic melanoma in the USA. *Melanoma Res* 2013; **23**:408–13.
6 Wee E, Wolfe R, McLean C *et al.* Clinically amelanotic or hypomelanotic melanoma: Anatomic distribution, risk factors, and survival. *J Am Acad Dermatol* 2018; **79**:645–51.
7 Gong HZ, Zheng HY, Li J. Clinicopathological characteristics and prognosis of amelanotic acral melanoma: a comparative study with pigmented acral melanoma. *Australas J Dermatol* 2020; **61**:358–61.
8 Farrell J, Stewart TJ, Rosen R. Study of clinical characteristics and risk factors for amelanotic/hypomelanotic melanoma in an Australian cohort. *Melanoma Res* 2022; **32**:129–30.
9 Vernali S, Waxweiler WT, Dillon PM *et al.* Association of incident amelanotic melanoma with phenotypic characteristics, MC1R status, and prior amelanotic melanoma. *JAMA Dermatol* 2017; **153**:1026–31.
10 Thomas NE, Kricker A, Waxweiler WT *et al.* Comparison of clinicopathologic features and survival of histopathologically amelanotic and pigmented melanomas: a population-based study. *JAMA Dermatol* 2014; **150**:1306–314.
11 Chamberlain AJ, Fritschi L, Kelly JW. Nodular melanoma: patients' perceptions of presenting features and implications for earlier detection. *J Am Acad Dermatol* 2003; **48**:694–701.
12 De Luca DA, Bollea Garlatti LA, Galimberti GN *et al.* Amelanotic melanoma in albinism: the power of dermatoscopy. *J Eur Acad Dermatol Venereol* 2016; **30**:1422–3.
13 Phan A, Touzet S, Dalle S *et al.* Acral lentiginous melanoma: a clinicoprognostic study of 126 cases. *Br J Dermatol* 2006; **155**:561–9.
14 Gualandri L, Betti R, Crosti C. Clinical features of 36 cases of amelanotic melanomas and considerations about the relationship between histologic subtypes and diagnostic delay. *J Eur Acad Dermatol Venereol* 2009; **23**:283–7.
15 Søndergaard K, Schou G. Survival with primary cutaneous malignant melanoma, evaluated from 2012 cases. A multivariate regression analysis. *Virchows Arch A Pathol Anat Histopathol* 1985; **406**:179–95.
16 Moon HR, Kang HJ, Won CH *et al.* Heterogeneous spectrum of acral melanoma: a clinicoprognostic study of 213 acral melanomas according to tumor site. *J Am Acad Dermatol* 2018; **78**:179–82.
17 Choi ME, Yang HJ, Won CH *et al.* Differences in the tumor immunity-related gene expression profile between acral lentiginous and non-acral melanoma. *J Am Acad Dermatol* 2023; **89**:411–13.
18 Merritt CR, Ong GT, Church SE *et al.* Multiplex digital spatial profiling of proteins and RNA in fixed tissue. *Nat Biotechnol* 2020; **38**:586–99.
19 Guo W, Yin G, Liu H *et al.* Matched analysis of the prognosis of amelanotic and pigmented melanoma in head and neck. *Acta Otolaryngol* 2020; **140**:785–8.
20 Wehbe M, Soudja SM, Mas A *et al.* Epithelial-mesenchymal-transition-like and TGFβ pathways associated with autochthonous inflammatory melanoma development in mice. *PLOS ONE* 2012; **7**:e49419.
21 Militaru IV, Rus AA, Munteanu CVA *et al.* New panel of biomarkers to discriminate between amelanotic and melanotic metastatic melanoma. *Front Oncol* 2022; **12**:1061832.
22 Ng MF, Simmons JL, Boyle GM. Heterogeneity in melanoma. *Cancers (Basel)* 2022; **14**:3030.
23 De Giorgi V, Gori A, Savarese I *et al.* Clinical and dermoscopic features of truly amelanotic plantar melanoma. *Melanoma Res* 2017; **27**:224–30.
24 Choi ME, Cho H, Won CH *et al.* Clinicopathologic characteristics of trauma-related nail apparatus melanoma: a comparative study according to the presence of trauma prior to melanoma development. *Dermatology* 2023; **239**:165–73.
25 Saibil H. Chaperone machines for protein folding, unfolding and disaggregation. *Nat Rev Mol Cell Biol* 2013; **14**:630–42.
26 Czarnecka AM, Campanella C, Zummo G *et al.* Mitochondrial chaperones in cancer: from molecular biology to clinical diagnostics. *Cancer Biol Ther* 2006; **5**:714–20.
27 Rappa F, Farina F, Zummo G *et al.* HSP-molecular chaperones in cancer biogenesis and tumor therapy: an overview. *Anticancer Res* 2012; **32**:5139–50.
28 Kabakov A, Yakimova A, Matchuk O. Molecular chaperones in cancer stem cells: determinants of stemness and potential targets for antitumor therapy. *Cells* 2020; **9**:892.
29 Lemieux P, Oesterreich S, Lawrence JA *et al.* The small heat shock protein hsp27 increases invasiveness but decreases motility of breast cancer cells. *Invasion Metastasis* 1997; **17**:113–23.
30 Sanderson S, Valenti M, Gowan S *et al.* Benzoquinone ansamycin heat shock protein 90 inhibitors modulate multiple functions required for tumor angiogenesis. *Mol Cancer Ther* 2006; **5**:522–32.
31 Calderwood SK, Theriault JR, Gong J. Message in a bottle: role of the 70-kDa heat shock protein family in anti-tumor immunity. *Eur J Immunol* 2005; **35**:2518–27.
32 Zhang T, Li Q, Zhang Y *et al.* Diagnostic and prognostic value of heat shock protein 90α in malignant melanoma. *Melanoma Res* 2021; **31**:152–61.
33 Shomali N, Hatamnezhad LS, Tarzi S *et al.* Heat shock proteins regulating Toll-like receptors and the immune system could be a novel therapeutic target for melanoma. *Curr Mol Med* 2021; **21**:15–24.
34 Pickart CM, Eddins MJ. Ubiquitin: structures, functions, mechanisms. *Biochim Biophys Acta* 2004; **1695**:55–72.
35 Takahashi Y, Ishii Y, Nishida Y *et al.* Detection of aberrations of ubiquitin-conjugating enzyme E2C gene (UBE2C) in advanced colon cancer with liver metastases by DNA microarray and two-color FISH. *Cancer Genet Cytogenet* 2006; **168**:30–5.
36 Hao Z, Zhang H, Cowell J. Ubiquitin-conjugating enzyme UBE2C: molecular biology, role in tumorigenesis, and potential as a biomarker. *Tumour Biol* 2012; **33**:723–30.
37 Kariri Y, Toss MS, Alsaleem M *et al.* Ubiquitin-conjugating enzyme 2C (UBE2C) is a poor prognostic biomarker in invasive breast cancer. *Breast Cancer Res Treat* 2022; **192**:529–39.
38 Liu Y, Zhao R, Chi S *et al.* UBE2C is upregulated by estrogen and promotes epithelial-mesenchymal transition via p53 in endometrial cancer. *Mol Cancer Res* 2020; **18**:204–15.
39 Zhang S, You X, Zheng Y *et al.* The UBE2C/CDH1/DEPTOR axis is an oncogene and tumor suppressor cascade in lung cancer cells. *J Clin Invest* 2023; **133**:e162434.
40 Di Trolio R, Simeone E, Di Lorenzo G *et al.* The use of interferon in melanoma patients: a systematic review. *Cytokine Growth Factor Rev* 2015; **26**:203–12.
41 Truitt ML, Ruggero D. New frontiers in translational control of the cancer genome. *Nat Rev Cancer* 2016; **16**:288–304.
42 Huang CI, Wang CC, Tai TS *et al.* eIF4E and 4EBP1 are prognostic markers of head and neck squamous cell carcinoma recurrence after definitive surgery and adjuvant radiotherapy. *PLOS ONE* 2019; **14**:e0225537.
43 Fabbri L, Chakraborty A, Robert C *et al.* The plasticity of mRNA translation during cancer progression and therapy resistance. *Nat Rev Cancer* 2021; **21**:558–77.
44 Sridharan S, Robeson M, Bastihalli-Tukaramrao D *et al.* Targeting of the eukaryotic translation initiation factor 4A against breast cancer stemness. *Front Oncol* 2019; **9**:1311.
45 Boussemart L, Malka-Mahieu H, Girault I *et al.* eIF4F is a nexus of resistance to anti-BRAF and anti-MEK cancer therapies. *Nature* 2014; **513**:105–9.

46 Zindy P, Berge Y, Allal B *et al*. Formation of the eIF4F translation-initiation complex determines sensitivity to anticancer drugs targeting the EGFR and HER2 receptors. *Cancer Res* 2011; **71**:4068–73.
47 Gong C, Tsoi H, Mok KC *et al*. Phosphorylation independent eIF4E translational reprogramming of selective mRNAs determines tamoxifen resistance in breast cancer. *Oncogene* 2020; **39**:3206–17.
48 Arozarena I, Wellbrock C. Phenotype plasticity as enabler of melanoma progression and therapy resistance. *Nat Rev Cancer* 2019; **19**:377–91.
49 Phung B, Ciesla M, Sanna A *et al*. The X-linked DDX3X RNA helicase dictates translation reprogramming and metastasis in melanoma. *Cell Rep* 2019; **27**:3573–86.
50 Liu J, Geng X, Hou J *et al*. New insights into M1/M2 macrophages: key modulators in cancer progression. *Cancer Cell Int* 2021; **21**:389.
51 Jairath NK, Farha MW, Jairath R *et al*. Prognostic value of intratumoral lymphocyte-to-monocyte ratio and M0 macrophage enrichment in tumor immune microenvironment of melanoma. *Melanoma Manag* 2020; **7**:MMT51.
52 Failing JJ, Yan Y, Porrata LF *et al*. Lymphocyte-to-monocyte ratio is associated with survival in pembrolizumab-treated metastatic melanoma patients. *Melanoma Res* 2017; **27**:596–600.
53 Ryu GW, Choi YD, Jin S *et al*. Volar location and degree of pigmentation are associated with poor survival and first metastasis pattern in acral melanoma. *Pigment Cell Melanoma Res* 2021; **34**:1094–104.